Journal of Hydraulic Research Vol. 46, No. 3 (2008), pp. 382–391
doi:10.3826/jhr.2008.2847

Parameters affecting water-hammer wave attenuation, shape and timing—Part 2: Case studies

Paramètres affectant l'atténuation, la forme et le retard du coup de bélier—Partie 2: Cas d'étude

ANTON BERGANT, (IAHR Member), *Litostroj E.I. d.o.o., 1000 Ljubljana, Slovenia. Tel.: +386 1 5824 284; fax: +386 1 5824 174; e-mail: anton.bergant@litostroj-ei.si (author for correspondence)*

ARRIS S. TIJSSELING, *Eindhoven University of Technology, P.O. Box 513, 5600 MB Eindhoven, The Netherlands. Tel.: +31 40 247 2755; fax: +31 40 244 2489; e-mail: a.s.tijsseling@tue.nl*

JOHN P. VÍTKOVSKÝ, (IAHR Member), *Department of Natural Resources and Water, Indooroopilly QLD 4068, Australia. Tel.: +61 7 3896 9134; fax: +61 7 3896 9898; e-mail: john.vitkovsky@nrw.qld.gov.au*

DÍDIA I.C. COVAS, *Instituto Superior Técnico, 1049-001 Lisboa, Portugal. Tel.: +351 21 8418 152; fax: +351 21 8418 150; e-mail: didia.covas@civil.ist.utl.pt*

ANGUS R. SIMPSON, (IAHR Member), *The University of Adelaide, Adelaide SA 5005, Australia. Tel.: +61 8 8303 5874; fax: +61 8 8303 4359; e-mail: asimpson@civeng.adelaide.edu.au*

MARTIN F. LAMBERT, (IAHR Member), *The University of Adelaide, Adelaide SA 5005, Australia. Tel.: +61 8 8303 5838; fax: +61 8 8303 4359; e-mail: mlambert@civeng.adelaide.edu.au*

ABSTRACT
This two-part paper investigates parameters that may significantly affect water-hammer wave attenuation, shape and timing. Possible sources that may affect the waveform predicted by classical water-hammer theory include unsteady friction, cavitation (including column separation and trapped air pockets), a number of fluid–structure interaction effects, viscoelastic behaviour of the pipe-wall material, leakages and blockages. Part 1 of this two-part paper presents the mathematical tools needed to model these sources. Part 2 of the paper presents a number of case studies showing how these modelled sources affect pressure traces in a simple reservoir-pipeline-valve system. Each case study compares the obtained results with the standard (classical) water-hammer model, from which conclusions are drawn concerning the transient behaviour of real systems.

RÉSUMÉ
Cet article, publié en deux parties, étudie les paramètres qui peuvent avoir un effet significatif sur l'atténuation, la forme et le retard de la variation de pression pendant un coup de bélier. Les phénomènes non considérés par la théorie classique du coup de bélier qui peuvent modifier la forme d'onde sont notamment la friction transitoire, la cavitation (y compris la séparation de la colonne et les poches d'air), l'interaction entre le fluide et la structure (FSI), le comportement viscoélastique du matériel de la conduite, les fuites et les blocages. La première partie de cet article présente les modèles mathématiques de calcul des effets de ces phénomènes. La deuxième partie présente une étude de cas qui illustre l'effet de ces phénomènes sur la variation de pression dans un système simple, composé d'un réservoir, d'une conduite et d'une valve. Dans l'étude de cas, les résultats obtenus sont comparés avec ceux du modèle classique du coup de bélier. Les conclusions sur le comportement réel des systèmes de conduites pendant le régime transitoire du coup de bélier sont tirées à partir de ces résultats.

Keywords: Air pocket, blockage, cavitation, column separation, fluid–structure interaction, leakage, unsteady friction, viscoelastic behaviour of the pipe-wall, water hammer

1 Introduction

A number of numerical case studies are presented to show how the effects of unsteady friction, cavitation (including column separation and trapped air pockets), fluid–structure interaction (FSI), viscoelastic behaviour of the pipe-wall, leakage and blockage change the water-hammer waveform predicted by classical theory. All these phenomena can be important and explain certain observations in field and laboratory. However, to identify these phenomena it is desirable to study their effects in the very same

Accepted on July 26, 2007/Open for discussion until December 31, 2008.

piping system. A simple reservoir-pipeline-valve system has been selected for clarity. The system is simulated using a standard water-hammer model based on Eqs (1) and (2) in Part 1 of this two-part paper, and a corresponding method of characteristics (MOC) numerical model that incorporates unsteady friction (for laminar and turbulent flow), cavitation (vaporous and gaseous), FSI (Poisson and junction coupling), viscoelastic behaviour of the pipe wall, leakage and blockage, or a combination of these, as described in Part 1. The objective of this paper is not to validate once again proven models, but to show and compare the effects of the different phenomena in a clear and simple way. The models that are used have been previously verified with measurements in a number of research publications:

(1) Unsteady friction model (Bergant *et al*., 2001; Vítkovský, 2001; Bergant *et al*., 2003a, 2003b; Vítkovský *et al*., 2006).
(2) Cavitation model (Wylie and Streeter, 1993; Bergant and Simpson, 1999; Bergant and Tijsseling, 2001).
(3) FSI model (Tijsseling *et al.*, 1996; Vardy *et al.*, 1996).
(4) Pipe wall viscoelastic model (Bergant *et al*., 2003a, 2003b; Covas *et al*., 2004, 2005).
(5) Leakage and blockage model (Vítkovský, 2001; Wang, 2002).

The standard water-hammer model is herein referred to as the 'classical model'.

1.1 Test pipeline system

The test system used for investigating water-hammer waveforms comprises a straight $L = 37.2$ m long sloping copper pipeline of $D = 22$ mm internal diameter and $e = 1.6$ mm wall thickness connecting two tanks (Fig. 1). For the numerical investigation of viscoelastic behaviour of the pipe-wall a medium-density polyethylene pipeline of the same dimensions is used instead of the copper pipeline. The pipe-wall is assumed to be hydraulically smooth. The test apparatus is equivalent to the experimental apparatus that is installed in the Robin Hydraulic Laboratory in the School of Civil and Environmental Engineering at the University of Adelaide (Bergant *et al.*, 2001).

The transient event is generated by the rapid closure of a downstream ball-type valve. The initial discharge in the case studies is $Q_0 = 0.076 \times 10^{-3}$ m^3/s (initial Reynolds number $Re_0 = 4360$) and the static head in tank 2 is $H_{T2} = 32$ m (pressure head difference between the two tanks is $\Delta h_{T2\to T1,0} = 0.14$ m); however, to obtain liquid column separation, $Q_0 = 0.114 \times 10^{-3}$ m^3/s ($Re_0 = 6540$) and $H_{T2} = 22$ m($\Delta h_{T2\to T1,0} = 0.26$ m) were used. The valve closure time for all cases is $t_c = 0.009$ s. The liquid wave speed a is 1319 m/s in the copper pipe and 231 m/s in the medium-density polyethylene pipe. The number of reaches in all numerical simulations is $N = 32$.

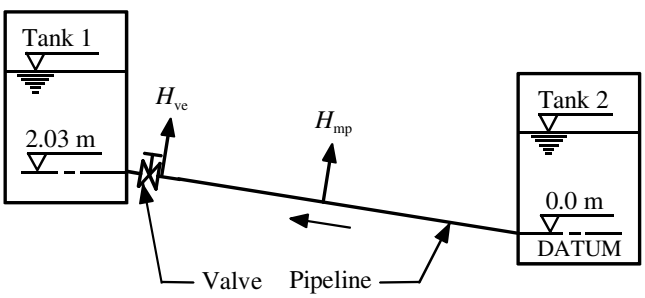

Figure 1 Test pipeline system (length $L = 37.2$ m; internal diameter $D = 22$ mm)

2 Unsteady friction

Traditionally the steady pipe flow friction approximation is incorporated in commercial water-hammer software packages. This assumption is satisfactorily applied to slow transients where the wall shear stress has a quasi-steady behaviour. Experimental validation of the steady friction model for rapid transients has shown significant deficiencies in attenuation, shape and timing of pressure waves (Bergant *et al*., 2001). The effect of unsteady friction on water-hammer waveforms is investigated using the copper pipeline shown in Fig. 1. Numerical results from the 'classical model' (steady friction) and the unsteady friction model (pure convolution-based model of Zielke (1968)) are compared. The Reynolds number of the initial flow (Re_0) is 4360 so that the initial flow is turbulent. The smooth-pipe turbulent Vardy–Brown weighting function (W_{app}) formulae are used (Vardy and Brown, 2003)—Fig. 2.

The results are compared at the valve (H_{ve}) and at the midpoint (H_{mp}) and are presented in Fig. 3. The simulations show that the steady friction approximation in the classical model underestimates the damping and dispersion predicted by the physically more correct unsteady friction model. Additionally, the steady friction model is not able to produce the evolution of the typical shape of the pressure oscillations, demonstrating its inability to model strong frequency-dependent attenuation.

3 Cavitation

The effect of vaporous and gaseous cavitation on the transient waveform is investigated for the configuration of the copper pipeline apparatus—see Fig. 1.

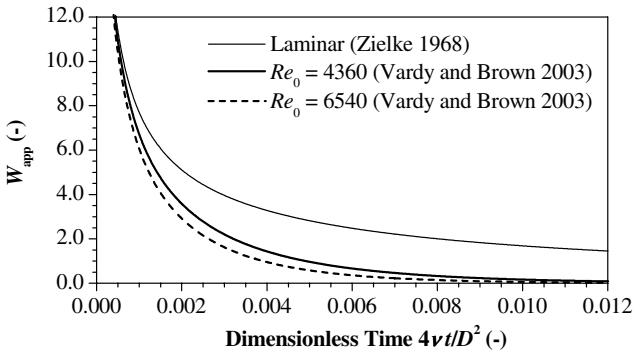

Figure 2 Weighting functions (W_{app}) for transient laminar flow (Zielke, 1968) and smooth-pipe turbulent flow (Vardy and Brown, 2003)

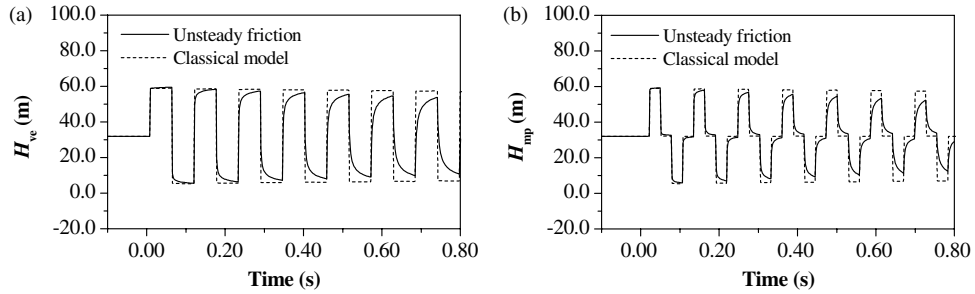

Figure 3 Results of unsteady friction model. Comparison of heads at the valve (H_{ve}) and at the midpoint (H_{mp}) in a copper pipeline; $Re_0 = 4360$

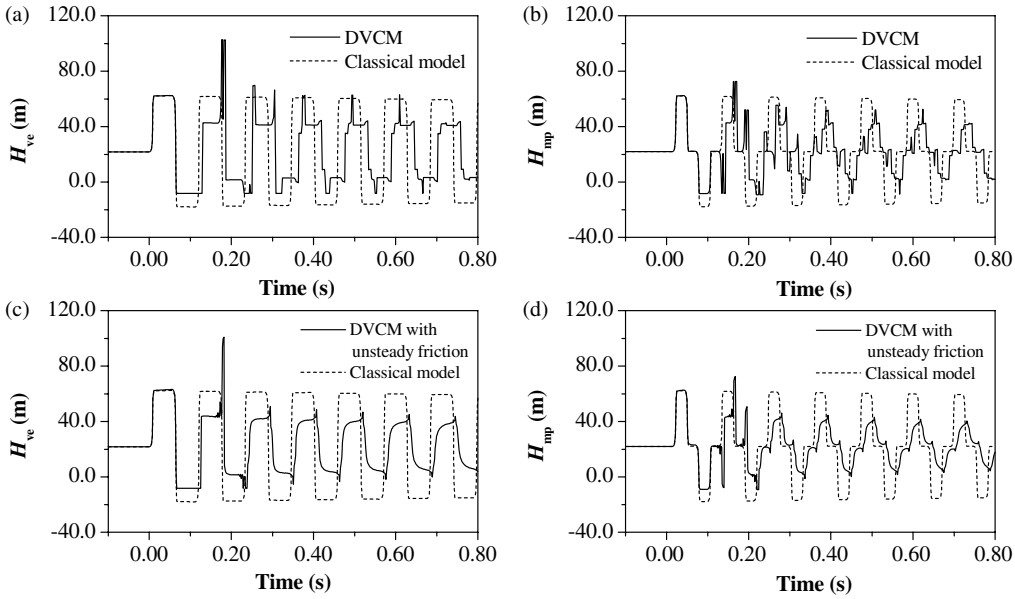

Figure 4 Results of DVCM. Comparison of heads at the valve (H_{ve}) and at the midpoint (H_{mp}) in a copper pipeline; $Re_0 = 6540$

3.1 Vaporous cavitation

Computational results are presented for the case with initial discharge $Q_0 = 0.114 \times 10^{-3}$ m^3/s. A weighting factor of $\psi = 1.0$ is used in the discrete vapour cavity model (DVCM) (Simpson and Bergant, 1994).

Computational results from the 'classical model' and the DVCM are compared at the valve (H_{ve}) and at the midpoint (H_{mp}) and are depicted in Fig. 4. The 'classical model' results (Fig. 4(a) and 4(b)) significantly differ from the DVCM (with steady friction) results. The actual flow situation concerns a column separation case with a maximum head significantly larger than the water-hammer head in pure liquid (at the valve - DVCM: $H_{ve,max} = 102.7$ m; 'classical model': $H_{ve,max} = 62.3$ m). The minimum pressure head predicted by the 'classical model' is well below the liquid vapour pressure head. The assumption of fluid homogeneity and continuity in the 'classical model' is violated when the pressure drops to the liquid vapour pressure. In this case, the liquid starts to vaporize and a large vapour cavity is formed at the valve. Some time after the first large cavity collapsed, a short-duration peak is super-imposed on the pressure head produced by the first cavity collapse.

A convolution-based unsteady friction model (Zielke, 1968) was incorporated into the DVCM to show the combined effects of vaporous cavitation and unsteady friction. The weighting function for the initial flow with a Reynolds number of 6540 was calculated using the Vardy–Brown weighting function (W_{app}) shown in Fig. 2. The results from the DVCM with unsteady friction are presented in Fig. 4(c) and 4(d). Although the bulk transient response remains the same, the inclusion of unsteady friction generates a significant damping of the pressure spikes.

3.2 Gaseous cavitation

Computational runs were performed using the discrete gas cavity model (DGCM) (Wylie, 1984; Wylie and Streeter, 1993) for two distinct flow situations:

(1) Gaseous cavitation in liquid with free gas present at all computational sections (simulation of pressure waves in bubbly flow).
(2) Trapped gas pocket at 13.95 m upstream of the valve (at the 3/8th point from the valve).

A weighting factor of $\psi = 1.0$ has been used in the DGCM (Wylie, 1984). Six different values of free gas void fraction (ratio of gas volume to total volume) $\alpha_{g0} = \{10^{-7}; 10^{-6}; 10^{-5}; 10^{-4}; 10^{-3}$ and $10^{-2}\}$ at atmospheric conditions were selected in the analysis for both flow situations (initial discharge $Q_0 = 0.076 \times 10^{-3}$ m^3/s). The aim of the analysis was

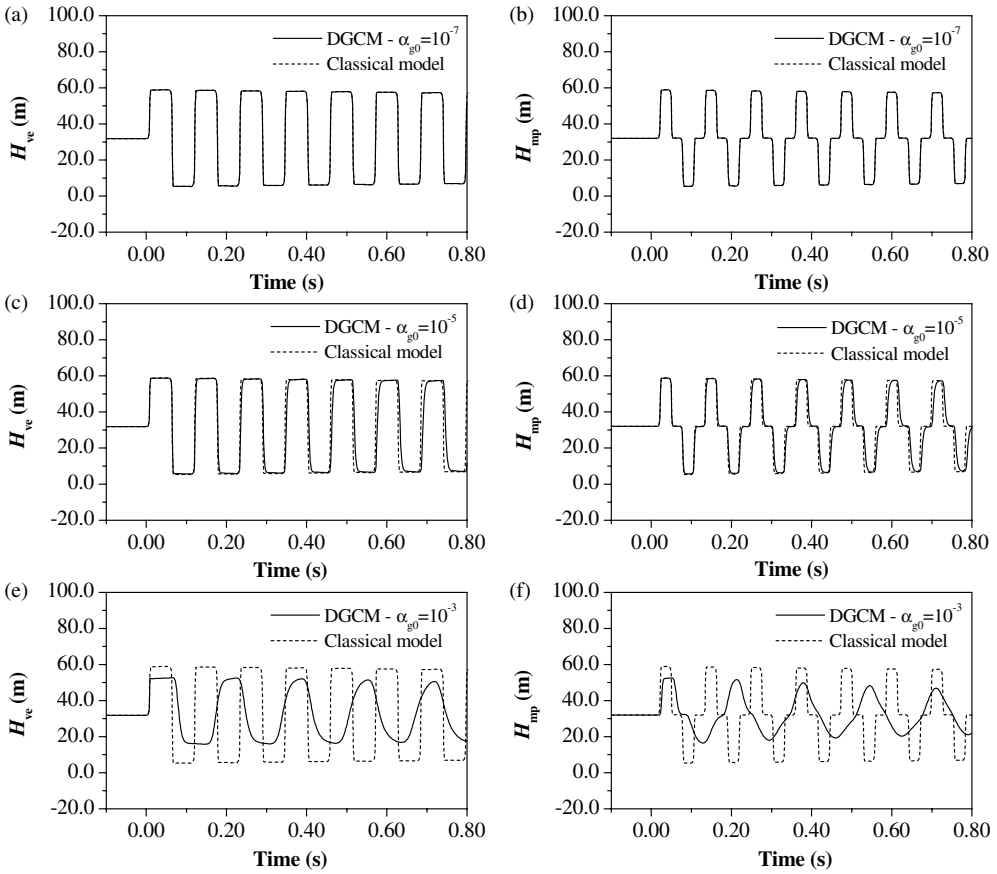

Figure 5 Results of DGCM. Comparison of heads at the valve (H_{ve}) and at the midpoint (H_{mp}) in a copper pipeline; $Re_0 = 4360$

to identify the effect of the amount of free gas on fluid transients. Computational results from the DGCM (with steady friction) are compared with 'classical model' results at the valve (H_{ve}) and at the midpoint (H_{mp}) and are depicted in Figs 5 and 6, respectively.

3.2.1 Liquid with free gas present at all computational sections

The DGCM results with a very low gas void fraction $\alpha_{g0} = 10^{-7}$ (Fig. 5(a) and 5(b)) perfectly match the 'classical model' results. The DGCM is capable of simulating water-hammer events in nearly 'pure' liquid. The DGCM results with a low gas void fraction $\alpha_{g0} = 10^{-5}$ (Fig. 5(c) and 5(d)) reveal a weak effect of small amounts of free gas. The discrepancies between the DGCM results and the 'classical model' results increase with increasing gas void fraction. Figure 5(e) and 5(f) display DGCM results with a large gas void fraction $\alpha_{g0} = 10^{-3}$. The actual flow situation represents a gaseous cavitation case with a maximum head significantly smaller than the water-hammer head (at the valve—DGCM: $H_{ve,max} = 52.6$ m; 'classical model': $H_{ve,max} = 58.9$ m).

3.2.2 Trapped gas pocket at the 3/8th point from the valve

In this case study, a single gas pocket is assumed to be trapped 13.95 m upstream of the valve (at the 3/8th point from the valve) in the copper pipeline. Six computational runs with void fractions of the trapped gas pocket $\alpha_{g0,3/8} = \{10^{-7}; 10^{-6}; 10^{-5}; 10^{-4}; 10^{-3}$ and $10^{-2}\}$ have been performed. The corresponding gas volume is still small in comparison to the total water volume. The DGCM has been used with a large void fraction at the 3/8th point and much smaller void fractions of 10^{-7} at the other computational sections.

A very small volume of the trapped gas pocket $\alpha_{g0,3/8} = 10^{-6}$ (Fig. 6(a) and 6(b)) does not visibly affect the pressure wave. The DGCM results with a small trapped gas pocket—$\alpha_{g0,3/8} = 10^{-4}$ (Fig. 6(c) and 6(d)) show a weak effect of the trapped pocket on the pressure traces. Longer simulations show that a beat develops. The discrepancies between the DGCM results and the 'classical model' results increase with increasing volume of the trapped gas pocket. Figure 6(e) and 6(f) present DGCM results with a large gas void fraction—$\alpha_{g0,3/8} = 10^{-2}$. In this case, the actual flow situation represents a gaseous cavitation case with a maximum head larger than the water-hammer head in 'pure' liquid (at the valve—DGCM: $H_{ve,max} = 67.7$ m; 'classical model': $H_{ve,max} = 58.9$ m).

4 Fluid–structure interaction

The test pipeline shown in Fig. 1 is used to theoretically study the possible effects of FSI. As a result, the 37.2 m long straight copper pipe ($E = 120$ GPa, $\rho_s = 8960$ kg/m^3, $\nu = 0.34$) is assumed not to be restrained against axial motion along its entire length. The tank at its upstream end is a fixed point, and the valve downstream (assumed to be of negligible mass) is either fixed or free to move, depending on the type of FSI under investigation. The pressure and axial stress wave speeds are taken

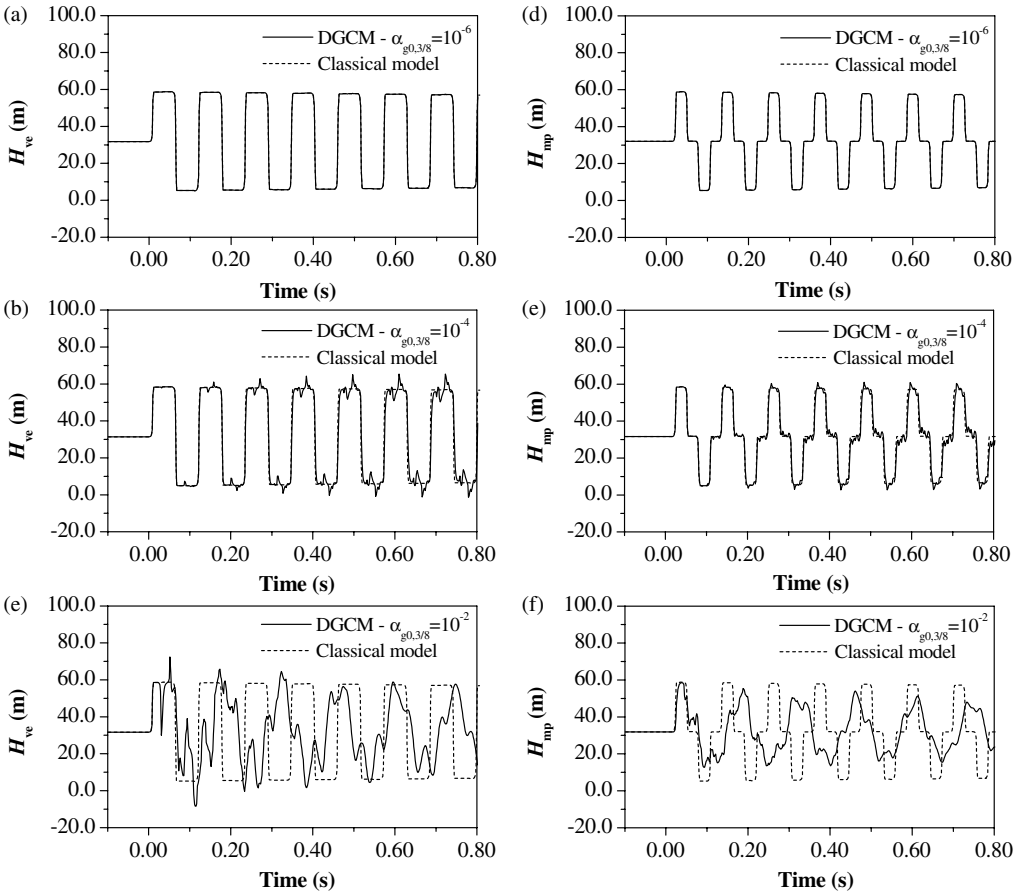

Figure 6 Results of DGCM with trapped gas pocket. Comparison of heads at the valve (H_{ve}) and at the midpoint (H_{mp}) in a copper pipeline; $Re_0 = 4360$

as $\tilde{a} = 1316.5\,\text{m/s}$ and $\tilde{a}_s = 3686.2\,\text{m/s}$, so that their ratio is 5/14. A non-staggered computational grid with $5 \times 32 = 160$ reaches, but with $\Delta t = 5\Delta x/\tilde{a}$, allows standard MOC calculation without interpolation (except for the boundary values needed at $\Delta t = \Delta x/\tilde{a}$ intervals) (Tijsseling and Lavooij, 1989). The effects of the different FSI mechanisms on the classical water-hammer waveform are demonstrated in the four cases below.

4.1 Poisson coupling

To study solely the effects of Poisson coupling (without friction), the valve is assumed to be fixed (immovable). Valve closure generates a travelling pressure rise, which radially expands the pipe wall. The radial expansion is accompanied with an axial contraction, which sends out a stress wave and an associated pressure change in the fluid (precursor). These effects are initially very small as can be seen from the pressure heads in Fig. 7(a) and 7(b): the first period of water hammer is not much affected by FSI. However, Fig. 7(a) and 7(b) also show that the effects cumulate to such an extent that unrealistically high and low pressures result. There is a continuous exchange and redistribution of energy between the water-hammer wave and the vibrating pipe. A beat phenomenon develops (Tijsseling, 1997). Precursor waves have been observed in laboratory experiments, but as far as the authors know, *Poisson-coupling beat* has not (although Fig. 4(a) of Budny *et al.* (1991) and Fig. 16 of Vennatrø (1999) exhibit cumulative Poisson coupling effects). Three obvious reasons are (i) unsteady friction and rubbing at pipe supports damp the transient event, (ii) pipe anchors never are entirely stiff or entirely inert when impact loaded, and (iii) pipes like to vibrate in their lowest and hence flexural mode, which is made possible through axial–lateral coupling at supports and bends.

4.2 Junction coupling

To study solely the effects of junction coupling (without friction), Poisson's ratio is set equal to zero so that the mechanisms described in the previous section do not exist. The valve is free to move now; it causes and follows the pipe vibration. The pressure rise generated by valve closure pushes the valve in the downstream direction, thereby creating additional storage for the fluid and as a result a lower initial pressure rise, Fig. 7(c) and 7(d). The fluid is not brought entirely to rest; it has the velocity of the valve. The axial stress wave generated by the movement of the valve travels to and from the upstream tank and at its return, after time $2L/\tilde{a}_s$, it pulls the valve back. This 'pumping' action explains the second pressure rise in Fig. 7(c) and 7(d). In contrast to the Poisson-coupling case, Fig. 7(a) and 7(b), junction coupling makes the pressure out of phase with classical water hammer, Fig. 7(c) and 7(d). The system becomes slower than the classical $4L/a$ system, mainly because $\nu = 0$ and $\alpha = 1$ in the FSI solution, and $\nu = 0.34$ and $\alpha = 0.87$ in the classical solution (see Part 1, Eq. (4)).

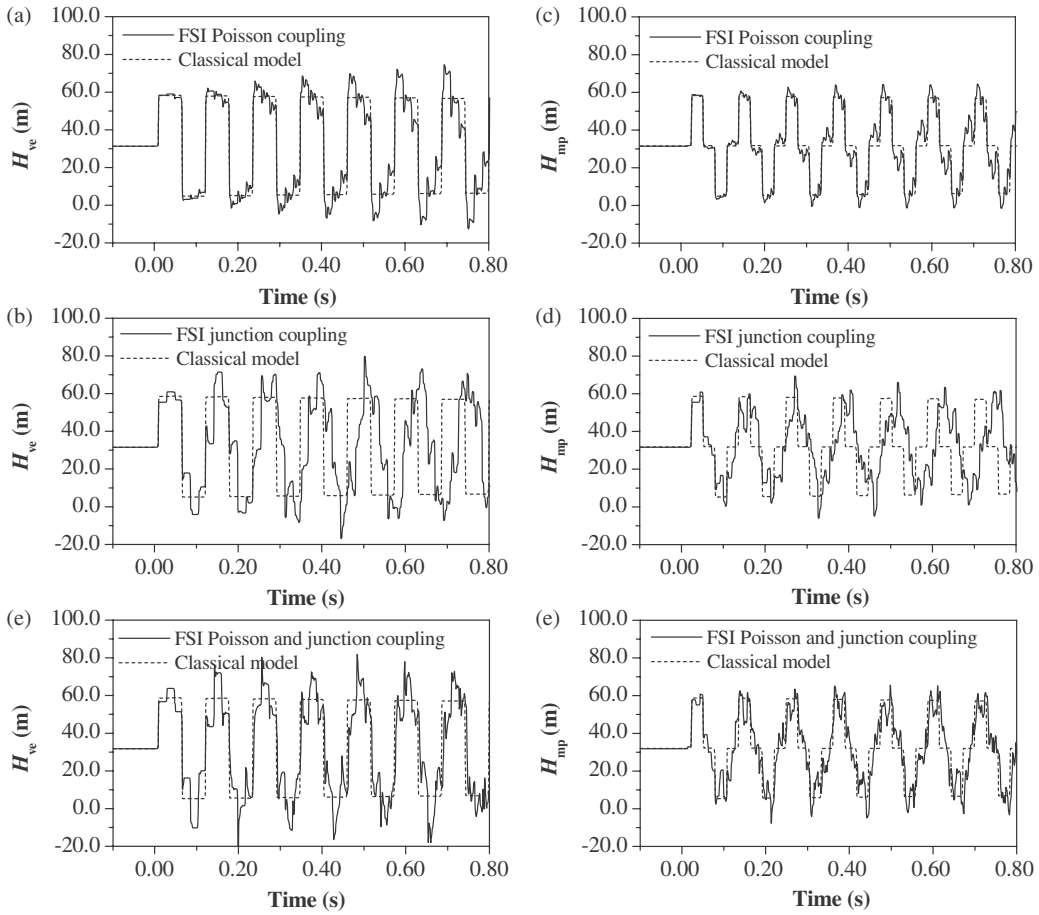

Figure 7 Results with FSI. Comparison of heads at the valve (H_{ve}) and at the midpoint (H_{mp}) in a copper pipeline; $Re_0 = 4360$

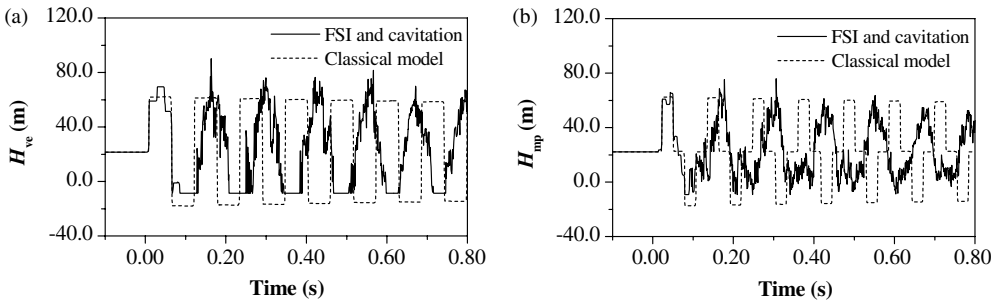

Figure 8 Results with FSI and cavitation (DVCM). Comparison of heads at the valve (H_{ve}) and at the midpoint (H_{mp}) in a copper pipeline; $Re_0 = 6540$

4.3 Poisson and junction coupling

Figure 7(e) and 7(f) show the combined effects of Poisson and junction coupling (without friction). Readers with good observational capability may be able to spot the precursor wave travelling ahead of the main water-hammer wave in Fig. 7(f). It is evident that FSI, when compared with the classical model, causes larger extreme pressures, high-frequency fluctuations, and a phase shift. It is noted that in multi-pipe systems with unrestrained elbows FSI may also cause, after one water-hammer period, a profound damping of the pressure wave as a consequence of water hammer-induced flexural pipe vibration (Erath *et al.*, 1999). FSI will not cause damping in unrestrained single-pipe systems.

4.4 FSI and cavitation

Figure 8 shows the combined effects of Poisson coupling, junction coupling, and vaporous cavitation (DVCM with steady friction). A large phase shift and high-frequency fluctuations are the most striking features. The subject of FSI and cavitation has been extensively dealt with in Tijsseling (1993).

5 Viscoelastic behaviour of the pipe wall

In this theoretical case study, the creep-compliance function taken from Gally *et al.* (1979) is for medium-density polyethylene at a temperature of 25°C and it is described by

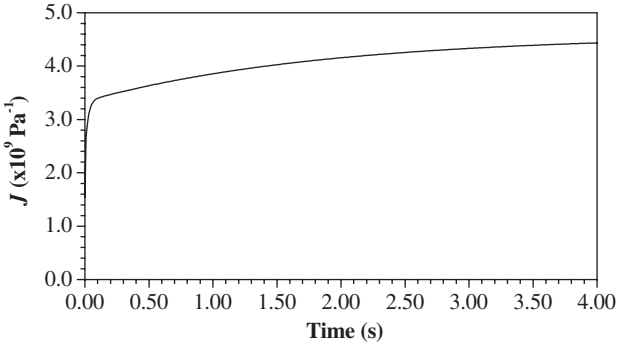

Figure 9 Creep-compliance function (J) for medium-density polyethylene (Gally *et al*., 1979)

a three-element Kelvin–Voigt model where $J_k = \{0.754 \times 10^{-9}, 1.046 \times 10^{-9}, 1.237 \times 10^{-9}\}\,\mathrm{Pa}^{-1}$ and $\tau_k = \{0.89 \times 10^{-4}, 0.0222, 1.864\}\,\mathrm{s}^{-1}$; $k = 1, 2, 3$. This creep-compliance function is shown in Fig. 9. The elastic component of the creep-compliance function corresponds to Young's modulus of elasticity $E = 0.649$ GPa. A constant Poisson's ratio is assumed as $\nu = 0.5$. The parameter α depends on the axial pipe constraints and is estimated to be $\alpha = 0.863$.

Figure 10(a) and 10(b) show the viscoelastic effect (with steady friction) on the pressure histories at valve and midpoint in the plastic pipeline (Fig. 1). The lower phase velocity, dispersion and higher attenuation are clear from the pressure responses. At the valve we see a lower pressure rise, except for the small initial peak that rapidly attenuates to a plateau. Figure 10(c) and 10(d) show the comparison of the classical response with the viscoelastic response with unsteady friction. The convolution-type unsteady friction model is used in combination with a smooth-pipe turbulent Vardy–Brown weighting function (W_{app}) for $Re_0 = 4360$ (Fig. 2). The numerical results in Fig. 10(c) and 10(d), when compared with the Fig. 10(a) and 10(b), show that the addition of unsteady friction has hardly any effect on the pressure response other than a slightly higher damping and dispersion of the pressure wave. This means that the effect of the viscoelastic behaviour of the pipe wall in the transient event, in this example, is dominant over unsteady friction. This phenomenon has been observed and discussed by Covas *et al*. (2004, 2005).

6 Discrete leakage and blockage

The effect of a leak and a blockage located 13.95 m upstream of the valve (at the 3/8th point from the valve) in the copper pipeline is now investigated (Fig. 1). Each pipeline fault was sized such that the steady-state ratios of leak flow to pipe flow, and of blockage head to reservoir head, were equal.

6.1 Discrete leakage

The leak has a diameter of 0.52 mm and a weighted area $C_d A_{\mathrm{Or}} = 15.25 \times 10^{-8}\,\mathrm{m}^2$. This gives a leak area to cross-sectional pipe area ratio of 0.056%. The ratio of the leak flow to the steady-state flow through the pipeline is 5%. Figure 11 shows the effect of the discrete leak on the pressure response at the valve and at the midpoint using both the steady friction model and the convolution-based unsteady friction model (Vardy and Brown, 2003). The presence of a leak increases the damping in the system. Additionally, the pressure response is more complicated due to reflections from the leak. The use of the convolution-based unsteady friction model damps the leak-induced reflections as the simulation time progresses, which is to be expected in a system where unsteady friction is dominant.

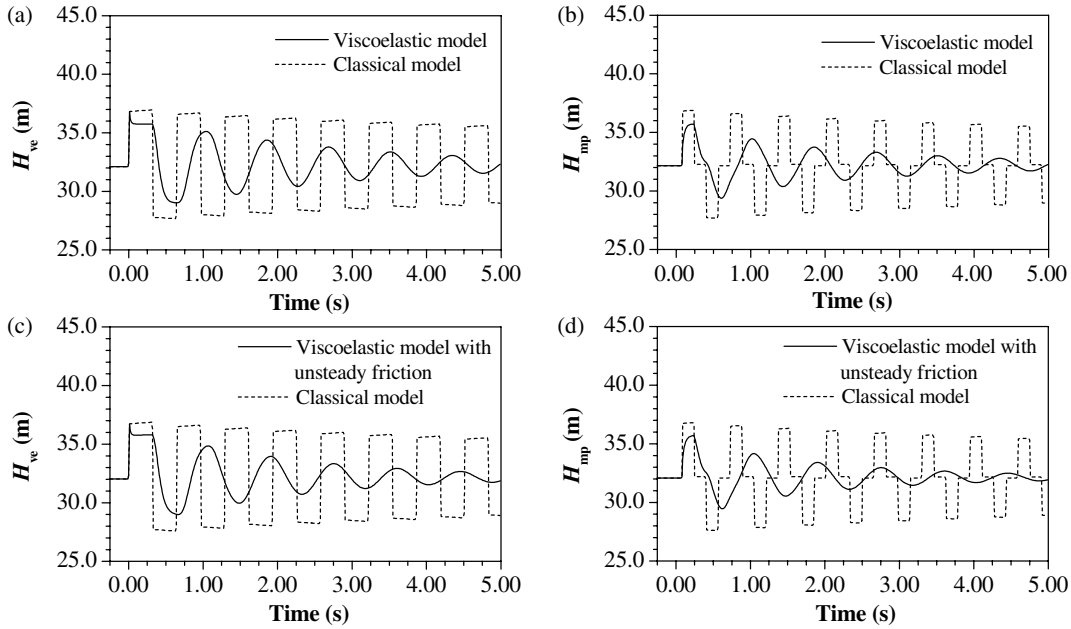

Figure 10 Results with viscoelastic pipe-wall. Comparison of heads at the valve (H_{ve}) and at the midpoint (H_{mp}) in a medium-density polyethylene pipeline; $Re_0 = 4360$

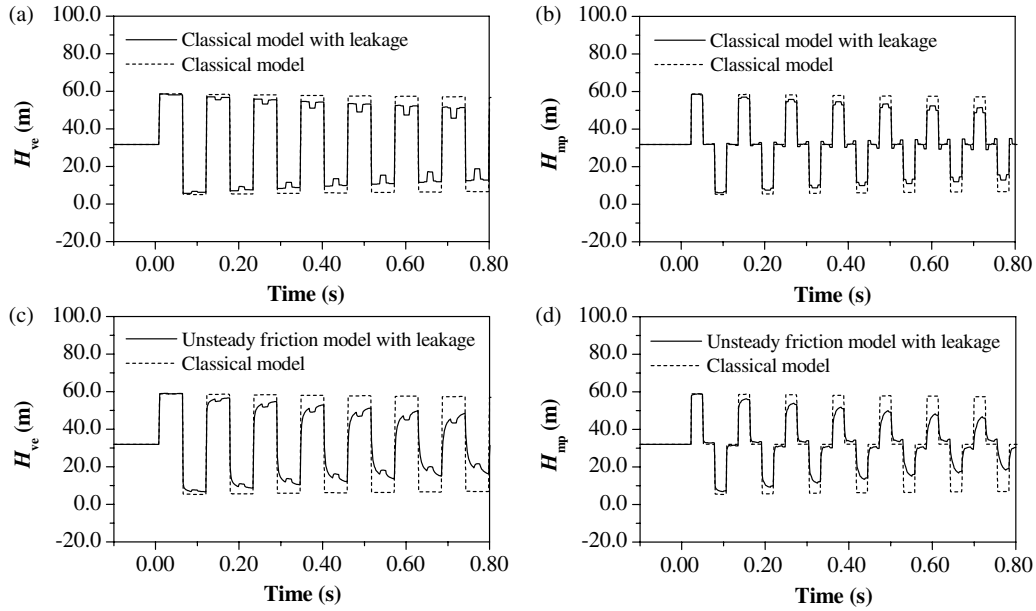

Figure 11 Results with leak. Comparison of heads at the valve (H_{ve}) and at the midpoint (H_{mp}) in a copper pipeline; $Re_0 = 4360$

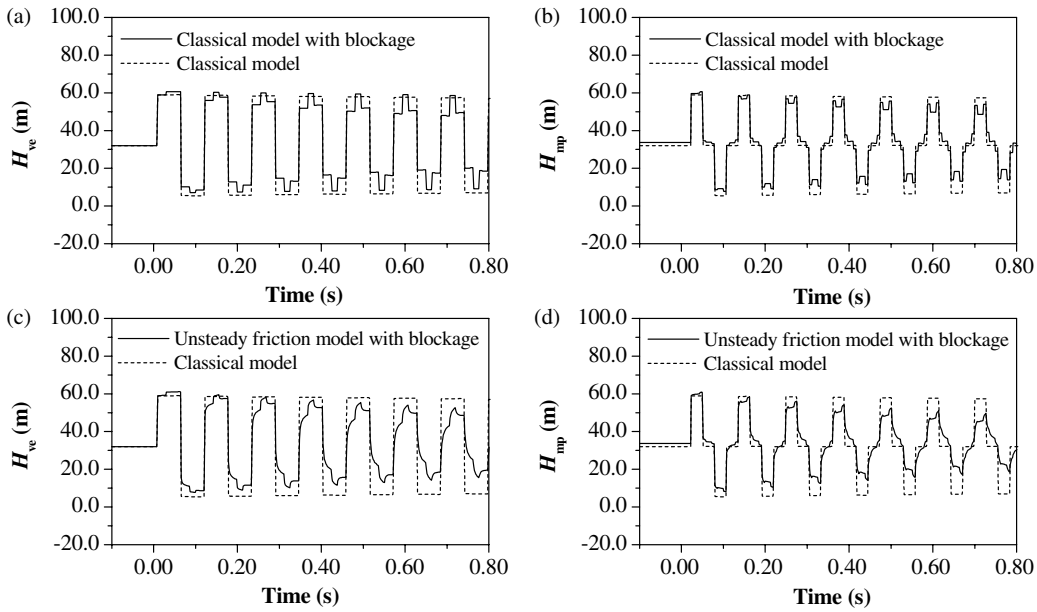

Figure 12 Results with blockage. Comparison of heads at the valve (H_{ve}) and at the midpoint (H_{mp}) in a copper pipeline; $Re_0 = 4360$

6.2 Discrete blockage

The blockage has a diameter of 4.94 mm and a weighted area $C_d A_{Or} = 1.33 \times 10^{-5}\,\mathrm{m}^2$ and it is located at the same position in the pipeline as the leak. This gives a blockage area to pipe area ratio of 5%. The ratio of the head loss across the blockage to the steady-state head in the pipeline is 5% (similar to leak flow). Figure 12 shows the pressure response for the blocked pipeline. Looking at the shape of the pressure response, the blockage effect is somehow the opposite of the leak effect. The inclusion of the unsteady friction model damps the reflections from the blockage.

The presence of leaks and blockages creates an attenuation of the pressure response with little dispersion. In this respect their effect is to damp and complicate the pressure response without significantly altering the phase of the response. The addition of unsteady friction in both cases accelerates the attenuation, making the leak- and blockage-induced pressure response shapes less defined. In both cases the leak and blockage contribute largely to the overall damping.

7 Conclusions

The presented case studies clearly show how the effects of unsteady friction, cavitation (including column separation and trapped air pockets), FSI, viscoelastic behaviour of the pipe wall, leakage and blockage change the water-hammer waveform in a simple reservoir-pipeline-valve system. Each case study concerns a classical water-hammer simulation and a corresponding MOC numerical model that incorporates each or a

combination of the aforementioned effects. The used models are simple and effective and could ideally be combined into one general model. The phenomena studied may cause additional damping (unsteady friction, bubbly flow, FSI in systems with laterally vibrating pipes, viscoelastic behaviour of the pipe-wall, leakage, blockage) or amplification (collapse of large vapour cavities, large trapped gas pockets, FSI) of the modelled transient traces. A beat phenomenon is predicted for FSI Poisson coupling and for small isolated air pockets. Because the analysed phenomena are not typically modelled in water-hammer software packages, but nevertheless are common in many hydraulic systems, it is important to be able to recognise them. The pressure traces presented herein can be used as a diagnostic tool for detecting faults and unexpected behaviour in the transient dynamics of liquid-filled pipe systems.

Notation

A_{Or} = Cross-sectional orifice area
a = Liquid wave speed
a_s = Solid wave speed
$\tilde{a}$ = FSI-modified wave speed
C_d = Orifice discharge coefficient
D = Internal pipe diameter
E = Young's modulus of elasticity of pipe-wall material
e = Pipe-wall thickness
H = Piezometric head
H_{T2} = Static head in tank 2 (Fig. 1)
J = Creep-compliance function
J_k = Kelvin–Voigt model parameter
L = Pipe length
N = Number of reaches
Q = Discharge
Re = Reynolds number ($Re = VD/\nu$)
t = Time
t_c = Valve closure time
V = Cross-sectionally averaged flow velocity
W = Weighting function for convolution-based unsteady friction model
α = Parameter dependent on the axial pipe constraints
α_g = Gas void fraction
$\Delta h_{T2\rightarrow T1}$ = Pressure head difference between tanks (Fig. 1)
Δt = MOC time step
Δx = MOC space step
ν = Kinematic viscosity; Poisson's ratio
ρ_s = Mass density of the pipe-wall material
τ_k = Retardation time in Kelvin–Voigt model
ψ = Weighting factor

Subscripts

app = Approximate
max = Maximum
mp = Midpoint
Or = Orifice
s = Structure, solid, pipe
ve = Valve
0 = Steady-state (initial) conditions

Abbreviations

DGCM = Discrete gas cavity model
DVCM = Discrete vapour cavity model
FSI = Fluid–structure interaction
MOC = Method of characteristics

Acknowledgement and disclaimer

The Surge-Net project is supported by funding under the European Commission's Fifth Framework 'Growth' Programme via Thematic Network 'Surge-Net' contract reference: G1RT-CT-2002-05069. The authors of this paper are solely responsible for the content and it does not represent the opinion of the Commission. The Commission is not responsible for any use that might be made of data herein.

References

Bergant, A., Simpson, A.R. (1999). Pipeline column separation flow regimes. *J. Hydraul. Eng. ASCE* 125(8), 835–848.

Bergant, A., Simpson, A.R., Vítkovský, J.P. (2001). Developments in unsteady pipe flow friction modelling. *J. Hydraul. Res. IAHR* 39(3), 249–257.

Bergant, A., Tijsseling, A.S. (2001). Parameters affecting water hammer wave attenuation, shape and timing. *Proceedings of the 10th International Meeting of the IAHR Work Group on the Behaviour of Hydraulic Machinery under Steady Oscillatory Conditions*, Trondheim, Norway, Paper C2.

Bergant, A., Tijsseling, A.S., Vítkovský, J.P., Covas, D., Simpson, A.R., Lambert, M.F. (2003a). Further investigation of parameters affecting water hammer wave attenuation, shape and timing—mathematical tools. *Proceedings of the 11th International Meeting of the IAHR Work Group on the Behaviour of Hydraulic Machinery under Steady Oscillatory Conditions*, Stuttgart, Germany, Paper 4.3.

Bergant, A., Tijsseling, A.S., Vítkovský, J.P., Covas, D., Simpson, A.R., Lambert, M.F. (2003b). Further investigation of parameters affecting water hammer wave attenuation, shape and timing—case studies. *Proceedings of the 11th International Meeting of the IAHR Work Group on the Behaviour of Hydraulic Machinery under Steady Oscillatory Conditions*, Stuttgart, Germany, Paper 4.4.

Budny, D.D., Wiggert, D.C., Hatfield, F.J. (1991). The influence of structural damping on internal pressure during a transient flow. *J. Fluids Eng. ASME* 113(3), 424–429.

Covas, D., Stoianov, I., Mano, J.F., Ramos, H., Graham, N., Maksimovic, C. (2004). The dynamic effect of pipe-wall viscoelasticity in hydraulic transients—experimental analysis and creep characterisation. *J. Hydraul. Res. IAHR* 42(5), 516–530.

Covas, D., Stoianov, I., Mano, J.F., Ramos, H., Graham, N., Maksimovic, C. (2005). The dynamic effect of pipe-wall viscoelasticity in hydraulic transients—model development, calibration and verification. *J. Hydraul. Res. IAHR* 43(1), 56–70.

Erath, W., Nowotny, B., Maetz, J. (1999). Modelling the fluid structure interaction produced by a waterhammer during shut-down of high-pressure pumps. *Nucl. Eng. Design* 193(3), 283–296.

Gally, M., Güney, M., Rieutord, E. (1979). An investigation of pressure transients in viscoelastic pipes. *J. Fluids Eng. ASME* 101(4), 495–499.

Simpson, A.R., Bergant, A. (1994). Numerical comparison of pipe-column-separation models. *J. Hydraul. Eng. ASCE* 120(3), 361–377.

Tijsseling, A.S., Lavooij, C.S.W. (1989). Fluid–structure interaction and column separation in a straight elastic pipe. *Proceedings of the 6th International Conference on Pressure Surges*, BHRA, Cambridge, UK, pp. 27–41.

Tijsseling, A.S. (1993). Fluid–structure interaction in case of waterhammer with cavitation. Ph.D. Thesis, Delft University of Technology, Faculty of Civil Engineering, Delft, The Netherlands. Available from: www.darenet.nl/en/page/language.view/search.page.

Tijsseling, A.S., Vardy, A.E., Fan, D. (1996). Fluid–structure interaction and cavitation in a single-elbow pipe system. *J. Fluids Struct.* 10(4), 395–420.

Tijsseling, A.S. (1997). Poisson-coupling beat in extended waterhammer theory. *Proceedings of the 4th International Symposium on Fluid–Structure Interactions, Aeroelasticity, Flow-Induced Vibration and Noise*, Dallas, USA, ASME - AD, 53-2, 529–532.

Vardy, A.E., Fan, D., Tijsseling, A.S. (1996). Fluid/structure interaction in a T-piece pipe. *J. Fluids Struct.* 10(7), 763–786.

Vardy, A.E., Brown, J.M.B. (2003). Transient turbulent friction in smooth pipe flows. *J. Sound Vibr.* 259(5), 1011–1036.

Vennatrø, R. (1999). Measurement of velocity profiles in water-hammer and steady oscillatory flow in a rigid steel pipe. *Proceedings of the 9th International Meeting of the IAHR Work Group on the Behaviour of Hydraulic Machinery under Steady Oscillatory Conditions*, Brno, Czech Republic, Paper C5.

Vítkovský, J.P. (2001). Inverse analysis and modelling of unsteady pipe flow: theory, applications, and experimental verification. Ph.D. Thesis, Department of Civil & Environmental Engineering, University of Adelaide, Adelaide, Australia.

Vítkovský, J.P., Bergant, A., Simpson, A.R., Lambert, M.F. (2006). Systematic evaluation of one-dimensional unsteady friction models in simple pipelines. *J. Hydraul. Eng. ASCE* 132(7), 696–708.

Wang, X.J. (2002). Leakage and blockage detection in pipelines and pipe networks. Ph.D. Thesis, Department of Civil & Environmental Engineering, University of Adelaide, Adelaide, Australia.

Wylie, E.B. (1984). Simulation of vaporous and gaseous cavitation. *J. Fluids Eng. ASME* 106(3), 307–311.

Wylie, E.B., Streeter, V.L. (1993). *Fluid Transients in Systems*. Prentice Hall, Englewood Cliffs, USA.

Zielke, W. (1968). Frequency-dependent friction in transient pipe flow. *J. Basic Eng. ASME* 90(1), 109–115.